Full Length Research Paper

Synthesis and preliminary characterization of polyethylene glycol (PEG)/hydroxyapatite (HAp) nanocomposite for biomedical applications

C. P. Dhanalakshmi[1], L. Vijayalakshmi[2] and V. Narayanan[1]*

[1]Department of Inorganic Chemistry, University of Madras, Guindy Maraimalai Campus, Chennai-600025, India.
[2]Department of Chemistry, S.D.N.B. Vaishnav College for Women, Chrompet, Chennai-600044, India.

Currently, composite materials have gained momentum in the field of orthopedics and maxillofacial surgery. Among the composite materials, ceramic/polymer possesses significant advantages of high mechanical reliability and excellent biocompatibility for applications in load bearing areas. In this work, polyethylene glycol (PEG)/hydroxyapatite (HAp) nanocomposites of varying weight percentages were synthesized and characterized physical-chemically by X-ray diffraction (XRD), Fourier transform infrared spectroscopy (FTIR), ^{31}P nuclear magnetic resonance (NMR), thermo gravimetric analysis (TGA), differential thermal analysis (DTA) and field emission-scanning electron microscopy (FE-SEM) and biologically by antimicrobial and anti-inflammatory assays to evaluate their potential use for biomedical applications. The results indicated that the size and crystallinity of HAp nanoparticles decrease with increase in PEG concentration in the composite. SEM confirmed the presence of HAp nanorod crystals in PEG matrix. The nano PEG-20/HAp demonstrated the highest antifungal and antibacterial activity and favorable inhibition of human cell hemolysis. The designed PEG/HAp nanocomposites constitute promising candidates for biomedical applications.

Key words: Hydroxyapatite, nanocrystalline, nanocomposite, poly ethylene glycol.

INTRODUCTION

The past three decades have witnessed a significant increase in the use of biomaterials for bone related surgical applications. In certain applications involving artificial bones and teeth, the thrust for high biocompatibility, bioactivity, ability for biodegradation and mechanical properties equivalent to bone and teeth is ensured from the clinical experience. Although, the present generation of biomaterials, like bioceramics and metallic alloys ensures for biocompatible and mechanical properties, respectively, this particular association mismatches with the original bone. In this way, a large variety of studies corroborate that performance of conjugated materials is better towards individual components, highlighting the importance of ceramic/ceramic and ceramic/polymer composites (Xiao et al., 2008). The calcium phosphate based bioceramics, particularly, hydroxyapatite (HAp) play an excellent role in biomedical applications owing to their excellent biocompatible, osteoconductive and bioactive properties, and its close chemical and physical resemblance to mineral component of bone tissue, enamel and dentin (Xiao et al., 2008). The major mineral phase of bone is HAp with a ratio of calcium-to-phosphate of 1.67 which was embedded as nano crystalline form in collagen triple helix structure (Bose and Saha, 2003). Currently, researchers are trying to mimic this natural nanocomposite system for tissue engineering applications. However, the brittleness and poor performance of mechanical stability of pure HAp limit its

---

*Corresponding author. E-mail: vnnara@yahoo.co.in. Tel: 91 44 22202793. Fax: 91 44 22300488.

use for the regeneration of non-load-bearing bone defects and tissue engineering applications (Ding et al., 2007). Composite biomaterials like metal and polymer matrix are used to improve the mechanical compatibility of nano HAp. Generally, composite biomaterials are prepared by using biocompatible/biodegradable and synthetic/natural polymers (Wang et al., 2007). Inorganic minerals such as HAp (Meenakshi et al., 2006), bioactive glasses (Rajendran et al., 2002), metal oxides (Ahn et al., 2002) and carbon nanotube (Singh et al., 2008) are incorporated into polymer matrixes to impart bioactivity. The addition of nanosized particles is desirable to develop composite with a good mechanical strength similar to the natural bone which contains mineral crystals at the nanometer scale and embedded in the collagen matrix (Joseph and Tanner, 2005; Yang et al., 1997). Polymer composites were designed to meet the specific requirement of biomedical applications like tissue engineering and drug delivery system. The right choice of the composition of both filler and polymer matrix are essential in addition to the processing method to obtain suitable biopolymer composites. Recently, attempts have been made to develop nanocomposites, wherein nano HAp particles are embedded in polyethylene glycol (PEG) polymeric matrices [Pramanik et al., 2006; Boissiere et al., 2006). Extensive studies have been made on both natural (collagen, gelatin and silk fibroin) and synthetic (polyethylene, polyamide, chitosan, polystyrene, poly[vinyl alcohol], poly[ethylene glycol/PEG] and poly[etheretherketone]) polymers to overcome the mechanical problems associated with bioceramics in bone tissue engineering applications (Li et al., 2009; Darder et al., 2006; Zhang and Mild, 2008). Among these different raw materials, PEG remains one of the widely used polymer group of biomaterials applied for medical implants. This usage is due to its segmented block co-polymer character. This wide range of versatility is utilized in terms of tailoring their applications, such as tissue scaffolding (Wiria et al., 2008), artificial cartilage (Pan and Xiong, 2009) and biodegradable scaffolds (Wang et al., 2008). In accordance to the related synergistic effect resulting from the combination of HAp and PEG, the present work describes the synthesis of a nanostructured HAp/PEG composite under controlled environment in varying compositions, evaluate their physical-chemical characteristics and discuss their biological potential as smart materials for biomedical applications.

EXPERIMENTAL DESIGN

Materials

The raw materials required to start the processing of the composite were: analytical grade calcium hydroxide ($Ca(OH)_2$) and ammonium dihydrogen phosphate ($(NH_4)H_2PO_4$) obtained from Merck (India), and PEG (MW 20000) purchased from Loba (India). Doubly distilled water was used as the solvent.

Methods

Synthesis of nano HAp

Nano HAp was synthesized by following a modified wet chemical method. At 25°C, 7.48 g of $Ca(OH)_2$ was first dissolved in a 100 ml volume of an ethanol-water mixture (50:50%, v/v) and was stirred for 3 h. A solution of 6.7 g $(NH_4)H_2PO_4$ was dissolved in 100 ml volume of water and then added to the $Ca(OH)_2$ solution over a period of 24 h. The amount of reagents in the solution was calculated to obtain a Ca/P molar ratio value equals 1.67, corresponding to a stoichiometric HAp. The pH of the slurry was measured digitally during the precipitation reaction, reaching a final value of pH 11.

Synthesis of PEG/HAp nanocomposites

The PEG/HAp nanocomposites were coded as nano PEG-20/HAp, nano PEG-40/HAp, nano PEG-60/HAp and nano PEG-80/Hap, where number denotes the weight (%) of PEG matrix (20,000) used in processing. Water was used as the solvent to prepare the polymer solution. PEG was dissolved by using magnetic stirrer for 3 h and the polymer solution was left overnight in room temperature to remove the air bubbles trapped in the viscous solution. Then, suitable amount of HAp was dispersed in deionized water by 30 min ultrasonication (METAL POWER ANALYTICAL (I) PVT. LTD. Maharashtra, India). Ultrasonication was necessary to avoid agglomeration of ceramic powder and to achieve proper dispersion. HAp in water was mixed with polymer solution under agitation. The homogeneously mixed solution is immediately taken to deep freeze (AC MAS Technology (p) Ltd, India) at -18°C. After 48 h freezing, the samples were freeze dried.

Physical-chemical characterization

The prepared samples were studied by Fourier transform infrared spectroscopy (FTIR) using a Schimadzu FT-IR 300 series instrument (Shimadzu Scientific Instruments, USA). The FTIR spectra were obtained over the region 450 to 4000 cm^{-1} in pellet form for 1 mg powder samples mixed with 200 mg spectroscopic grade (KBr). Spectra were recorded at 4 cm^{-1} resolution averaging 80 scans. The structure of the samples were analyzed by X-ray diffraction (XRD) using a Rich Siefert 3000 diffractometer (Seifert, Germany) with Cu-Kα_1 radiation (λ = 1.5418 Å). Diffraction peak at 25.9° was chosen for calculation of the crystallite size by Scherrer's formula since it is sharper and isolated from others. This peak assigns to (002) Miller's plane family and shows the crystal growth along the axis of HAp crystalline structure. The morphology of the materials was analyzed by field emission-scanning electron microscopy (FE-SEM) using a HITACHI S600N scanning electron microscopy (HITACHI High Tech, Japan). For the elemental analysis, the electron microscope was equipped with an energy dispersive X-ray attachment (EDAX). Thermo gravimetric analysis (TGA) coupled with differential thermal analysis (DTA) of the material was performed (STA 1500, PL Thermal Science) between 35 and 1400°C in air at a heating rate of 20K per minute to monitor the weight loss of organic residues. ^{31}P-MAS-NMR spectra were recorded on a Bruker MSL 300 spectrometer (HORIBA Scientific USA) equipped with an Andrew type rotor rotating at a frequency of 10 KHz.

Antimicrobial characterization

Inoculums preparation was used in the antifungal activity test of the human pathogenic fungus from American Type Culture Collection

(ATCC, USA) *Candida albicans* (ATCC 90028) and *Candida paratropicalis* (ATCC 42618). In the antibacterial susceptibility test, fresh bacterial colonies from ATCC (USA) of the five pathogenic strains (*Staphylococcus aureus* [ATCC 12600], *Escherichia coli* [ATCC 11775], *Salmonella typi* [ATCC 700931], *Vibrio cholerae* [ATCC 39315] and *Klebsiella pneumonia* [ATCC 13883]) were inoculated to Tryptic soy or Brain Heart Infusion broth (EMD chemicals USA) and was incubated at 37°C during a time period of 22 to 24 h. Turbidity was adjusted with sterile broth so as to correspond to the McFarland 0.5 barium sulfate method, where the standard is equivalent to 1.5×10^6 Colony Forming Units (CFU)/ml in a 1:100 dilution of a suspension of turbidity. This is prepared by adding 0.5 ml of 1.175% w/v (0.048 m) hydrate ($BaCl_2.2H_2O$) to 99.5 ml of 1% w/v (0.36) sulfuric acid (Merk, India).

Antifungal and antibacterial activities of the PEG/HAp nanocomposites were tested by the well diffusion method using Sabouraud dextrose agar and Muller Hinton agar (Sigma Aldrich, India). The radial growth of the colony was analyzed on completion of the incubation, and the mean diameter for each composite at a concentration of 250, 500, 750 and 1000 µg/ml were recorded. The average percentage inhibition of the bacterial growth medium was compared using the Vincent equation $I = 100/(C-T)/C$, where: I = percentage inhibition, T = average diameter of the bacterial growth on the tested plates and C = average diameter of the growth on the control plates. Stock solutions of tested compounds were prepared in dimethyl sulfoxide (Sigma-Aldrich, India).

***Anti-inflammatory activity test by HRBC membrane stabilization method***

The human red blood cells (HRBC) membrane stabilization has been used as a method to study the anti-inflammatory activity. After approbation of Human Research Ethics Committee and signed consent form, blood samples collected from healthy volunteer were used in this test. The harvested blood was mixed with equal volume of sterilized Alsever solution (2% dextrose, 0.8% sodium citrate, 0.05% citric acid and 0.42% sodium chloride in water). The blood was centrifuged at 3000 rpm and packed cell were washed with isosaline (0.85%, pH 7.2) and a 10% (v/v) suspension was made with isosaline. The assay mixture contained the drug (various concentrations (g/ml)), 1 ml of phosphate buffer (0.15 M, pH 7.4), 2 ml of hyposaline (0.36%) and 0.5 ml of HRBC suspension. Diclofenac (Sigma Aldrich, India) was used as reference drug. Instead of hyposaline, 2 ml of distilled water was used in the control. All the assay mixtures were incubated at 37°C for 30 min and was centrifuged. The hemoglobin content in the supernatant solution was estimated using spectrophotometer at 560 nm (Shimadzu Scientific Instruments, USA). The percentage protection was calculated by assuming the hemolysis produced in the presence of distilled water as 100%. The percentage of haemolysis was calculated using the formula:

$$\text{Protection (\%)} = \frac{100 - \text{Optical density of drug treated sample}}{\text{Optical density of control}} \times 100$$

RESULTS AND DISCUSSION

XRD analysis

The XRD patterns of nano HAp and nano PEG/HAp composites were taken. The patterns indicate the presence of amorphous HAp. The broad peaks reveal
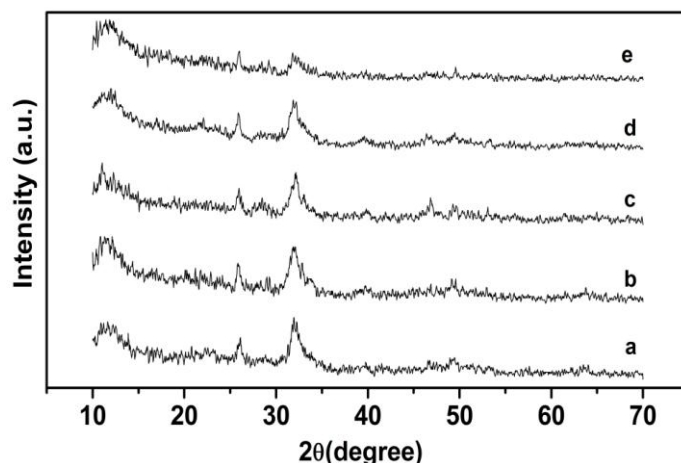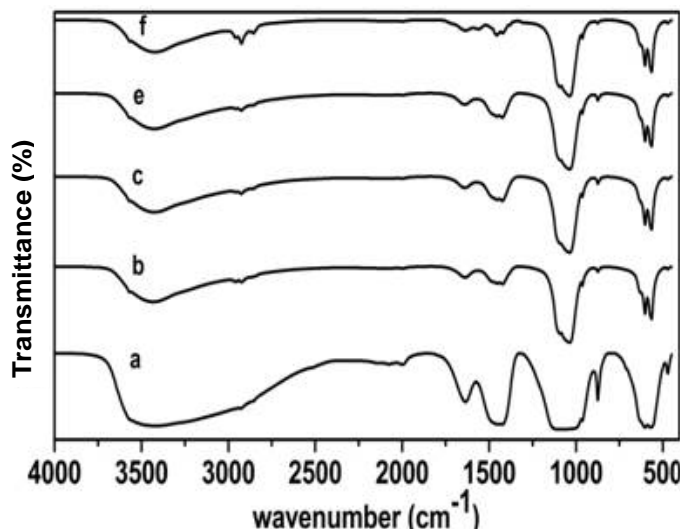

Figure 1. XRD pattern of (a) nano HAp, (b) nano PEG-20/HAp, (c) nano PEG-40/HAp, (d) nano PEG-60/HAp and (e) nano PEG-80/Hap.

that the particles sizes are very small in the range of 35 to 50 nm. The reflection planes corresponding to the characteristic XRD spectral peaks of pure nano HAp and PEG/HAp nanocomposites are as shown in Figure 1. The observed diffraction peaks were identified by standard Joint Committee on Powder Diffraction Standards (JCPDS) file (no. 09-0432) and are assigned as crystalline HAp. The XRD patterns show diffraction peaks with line broadening and high intensities, which confirms the nanosize with crystalline nature. The diffraction peaks, particularly in the planes 002, 211, 112 and 300 are high and narrow implying that the HAp crystallizes well. The crystallite size of the pure HAp and PEG/HAp composite was calculated using Scherrer's formula (Chen et al., 2004). Figure 1 reveals that the crystallite size decreases with increase in the composition of PEG (Kannan et al., 2006).

FTIR analysis

The FTIR spectra of pure nano HAp and nano PEG/HAp composites are as shown in Figure 2. The v_2 phosphate stretching mode that appeared at 471 to 472 cm^{-1} corresponds to PO_4^{3-} group in HAp (Degirmenbasi et al., 2006). The bands located at 1032 to 1048 and 562 to 570 cm^{-1} are attributed, respectively to the v_3 and v_4 P-O vibration modes of regular tetrahedral PO_4^{3-} groups (Yanbao et al., 2008). The observed band at 602 cm^{-1} corresponds to O-P-O bending and v_1 symmetric P-O stretching modes (Ma et al., 2006). The v_1 symmetric stretching mode of phosphate group was observed at 962 cm^{-1} (Zhang et al., 2003). The observed bands at 1384 cm^{-1} is due to the stretching mode of carbonate, which may be due to the acquisition of air during mineral precipitation (Bertinetti et al., 2007). Similarly, the

Figure 2. FTIR spectrum of (a) nano HAp, (b) nano PEG-20/HAp, (c) nano PEG-40/HAp, (e) nano PEG-60/HAp and (f) nano PEG-80/HAp.

observed bands at 1416 and 857 to 874 cm^{-1} were assigned to carbonate ions (Choi et al., 2006). The bands observed in the region between 2067 and 2069 cm^{-1} were related to their harmonic overtones and/or combination bands (Neira et al., 2009). The lattice H_2O exists in the range of 1603 to 1608 cm^{-1}, while the bands observed at 3400 to 3569 cm^{-1} overlap the –OH group (Kannan and Ferreira, 2006; Lak et al., 2008). The band observed between 2942 and 2944 cm^{-1} corresponds to C-H stretching band of PEG (Murugan and Ramakrishna, 2004). A new peak of stretching band was observed at 2944 cm^{-1}, when the PEG was added. This indicates that the chemical bond interactions between HAp and PEG (Pramanik et al., 2008).

FE-SEM analysis

SEM images of pure nano HAp and different weight percentages of PEG compositions are as shown in Figure 3. The SEM picture shows that particles exhibit nano rod morphology. The particle size of pure HAp is 27 nm. In case of composites, when the composition of PEG is added to HAp, the rod-like morphology starts to disappear. Increase in the PEG compositions that is, 20, 40 and 60 wt% leads to a corresponding change from rod-like to an irregular morphology. Furthermore, it is evident that the particle size increases with increase in PEG composition. The elemental analysis (EDAX) of nano PEG-20/HAp and nano PEG-60/HAp can demonstrate similar composition as shown in Figure 4. Mineral composition (calcium phosphate: Ca, O and P) and organic content (C) are present in both nanocomposites tested.

Thermo gravimetric analysis

The TGA (Figure 5) of the PEG/HAp nanocomposites powder was carried out between 50 and 1400 °C in air at a heating rate of 20°C min^{-1}. The decomposition behaviour of PEG/HAp nanocomposite is as shown in Figure 5. The nano HAp content was calculated from the residual weight in TGA curves at 600°C. However, since it is very difficult to control adsorbed water content in the composites, this nano HAp content is only an approximate value. In the TGA curves, several steps were observed. The first step, showing a small decrease in weight, is associated with adsorbed water-removing when heated above 90°C. The second step from 200 to 280°C may be due to the dehydration reaction of C-OH groups in PEG chains. This temperature shifts to a higher temperature, when the nano HAp content increases. The third step was degradation of PEG matrix releasing CO_2 gas. This temperature shifts to a lower temperature in the TG curves caused by the increasing nano HAp content. The fact that the second step was initiated at slightly higher temperature and the third step occurs at slightly at lower temperature than in pure PEG is suggestive of the presence of chemical interaction between PEG and the nano HAp.

^{31}P MAS-NMR analysis

The ^{31}P MAS-NMR spectra for the PEG/HAp nanocomposite and nano HAp powders are as shown in Figure 6. A distinctive resonance peak appears at 2.568 ppm in Figure 6a for the nano HAp. After the development of PEG/HAp nanocomposites, the ^{31}P characteristic peak moves to 2.645 ppm as shown in Figure 6b, indicating that after the formation of nanocomposites, the chemical environment of the phosphorus atom in nano HAp crystal has been changed. This shift is due to the interaction of HAp with PEG in PEG/HAp nanocomposite. The chemical interaction may be due to the hydrogen bonding interaction between the PO_4^{3-} ions of HAp and the –OH functional groups of PEG (Zhan et al., 2005).

Antimicrobial analysis

The antifungal activities of the screened data for the composites are given in Table 1. It was observed from the results that PEG/HAp nanocomposites shows some antifungal activity. However, the PEG-20/HAp nanocomposite showed higher activity against the tested fungus at concentration of 1000 µg/ml and other inoculums dilutions when compared with the other PEG/HAp nanocomposite.

When the antibacterial activity was evaluated, as shown in Table 1, all the PEG/HAp compositions of nanocomposite showed comparable activity against all
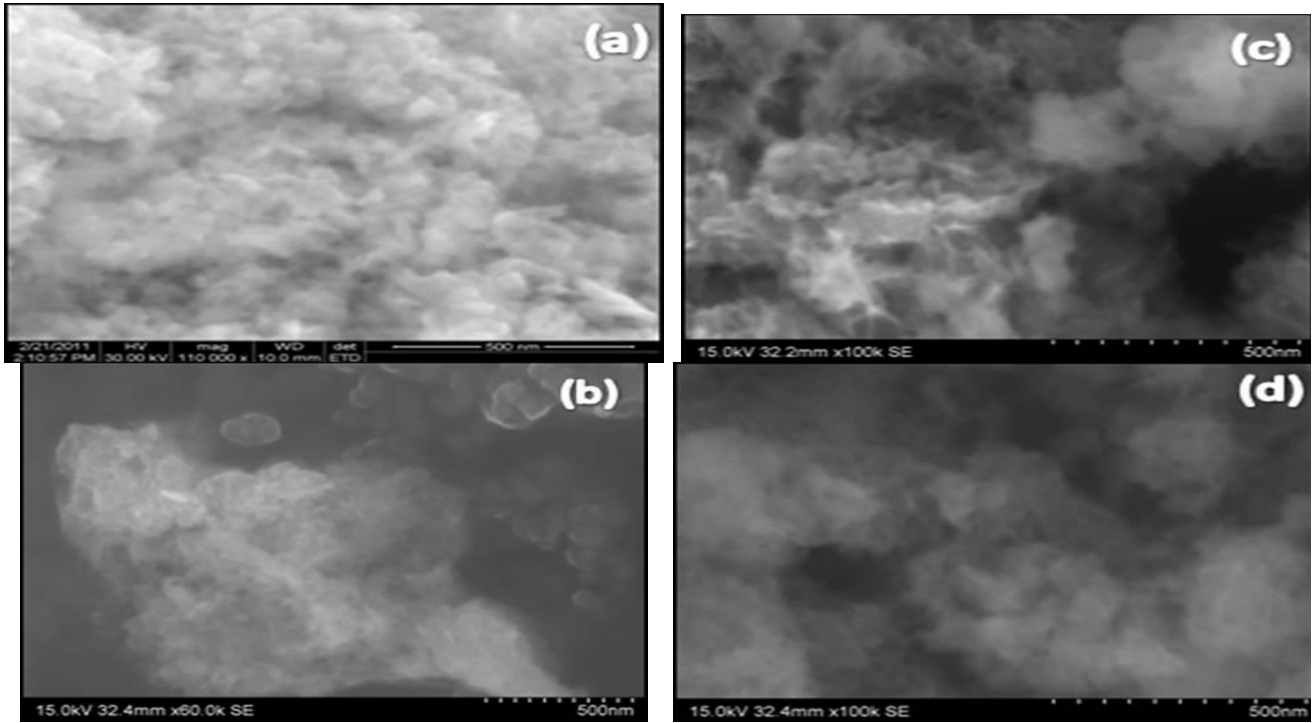
Figure 3. FE-SEM images of (a) nano HAp, (b) nano PEG-20/HAp, (c) nano PEG-40/HAp and (d) nano PEG-60/Hap.
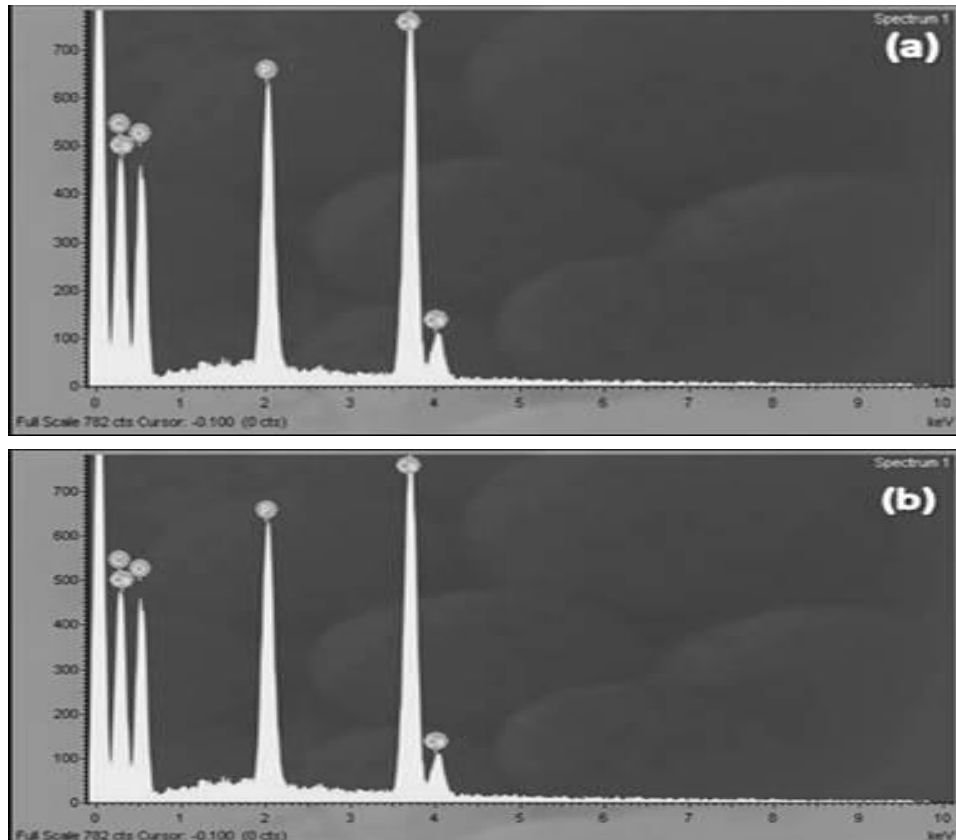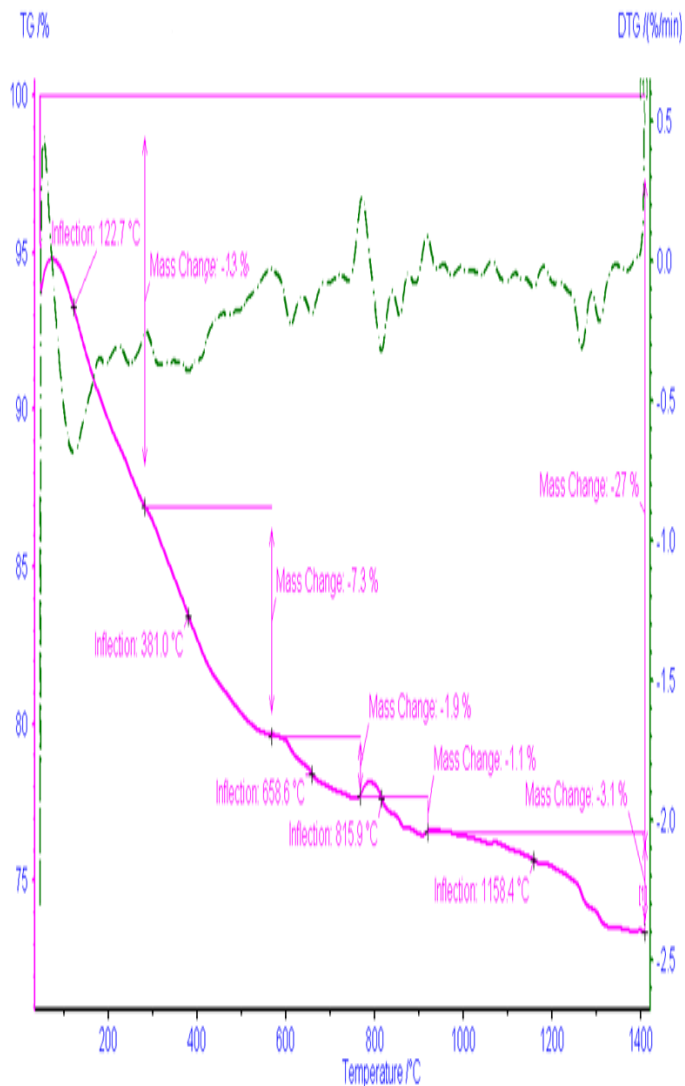

Figure 4. EDAX spectrum of (a) nano PEG-20/HAp and (b) nano PEG-60/Hap.

Figure 5. TGA curve of nano PEG-20/HAp composite.

the selected bacteria. From the data, it was observed that at a concentration of 1000 µg/ml, the composite of PEG-40/HAp showed higher antibacterial activity against *S. typi, V. cholera, E. coli* and *K. pneumoniae*. PEG-20/HAp showed higher antibacterial activity against *S. aureus*. PEG-60/HAp showed higher antibacterial activity against *E. coli*. PEG-80/HAp also showed higher antibacterial activity against *S. typi* and *K. pneumonia*. The antibacterial activity is dependent on the molecular structure of the compound, the solvent used and the bacterial stain under consideration.

Anti-inflammatory potential analysis

The compound, PEG-20/HAp and PEG-60/HAp showed
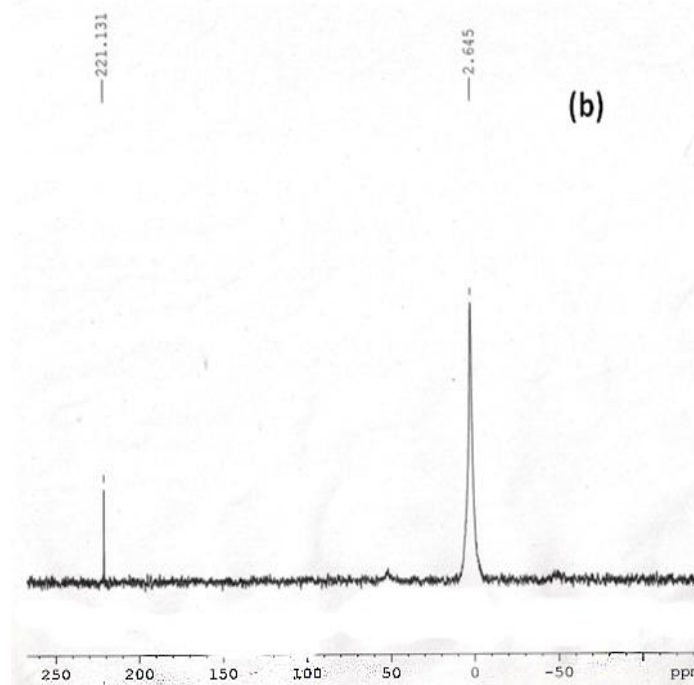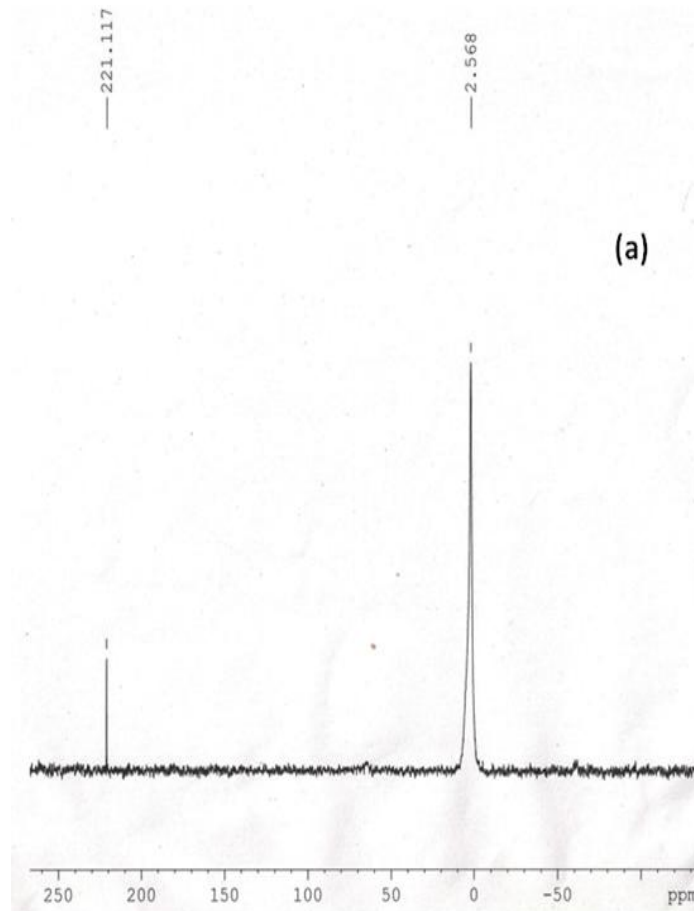
Figure 6. ^{31}P MAS-NMR spectra of (a) nano HAp and (b) nano PEG-40/HAp composite.

Table 1. Antibacterial and antifungal activity of nano PEG/HAp nanocomposites.

Organism	Sample name (Representation of zone of inhibition (diameter in mm))											
	nano PEG-20/HAp			nano PEG-40/HAp			nano PEG-60/HAp			nano PEG-80/HAp		
	Concentration (µg)			Concentration (µg)			Concentration (µg)			Concentration (µg)		
	500	750	1000	500	750	1000	500	750	1000	500	750	1000
S. aureus	11	12	13	11	11	11	11	11	11	-	-	-
S. typi	-	11	12	13	14	15	12	13	13	13	14	14
E. coli	-	11	12	13	13	14	11	13	14	11	12	13
V. cholerae	11	12	11	11	12	14	-	-	11	11	12	-
K. pneumoniae	-	12	12	11	15	17	12	11	11	-	12	15
C. albicans	11	12	13	-	11	12	-	11	12	11	11	12
C. paratropicalis	11	12	12	-	11	12	-	11	11	-	11	11
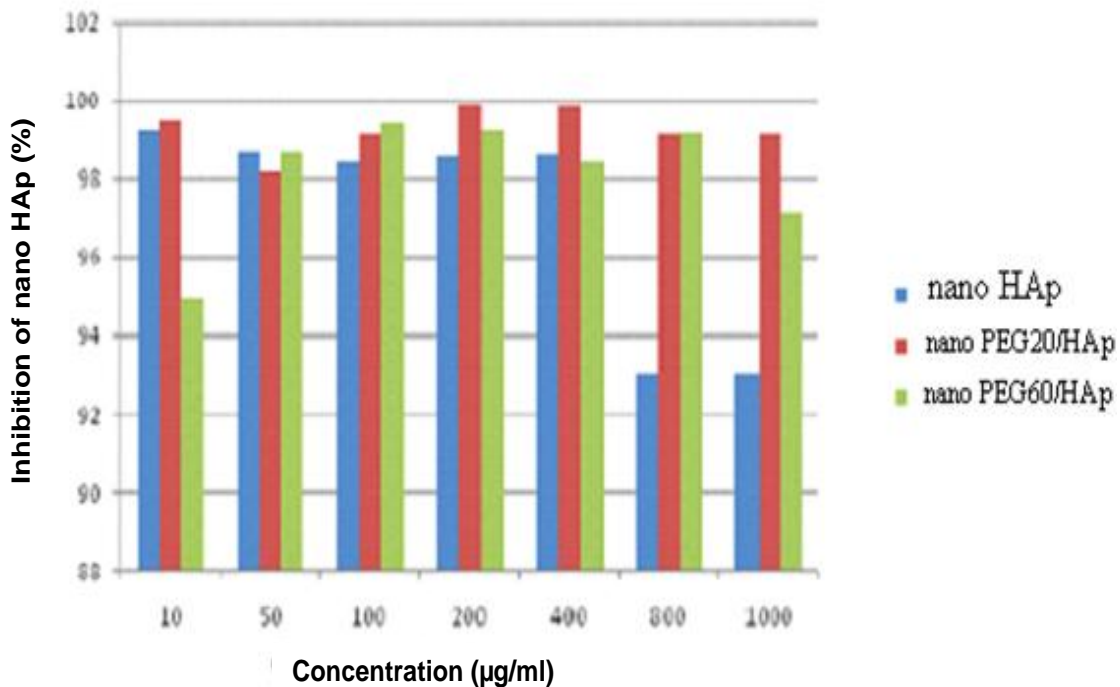
Figure 7. Anti-inflammatory activities of nano HAp and its composite.

significant protection towards HRBC membrane rupture which was induced by hypotonic saline. The effect may be due to the resistance caused by polymers in the destruction of erythrocyte membrane. From the results, it was proved that nano PEG-20/HAp composition was more effective than nano PEG-60/HAp composition and also nano HAp (Figure 7 and Table 2). Further work is in progress to identify the exact mechanism involved in anti-inflammatory activity. A challenge in regenerative medicine is to develop a biomaterial with good mechanical and biological properties and with perspective to act as a cell carrier of stem cells or differentiated cells.

Conclusions

In the present work, a novel PEG/HAp nanocomposite was prepared by simple chemical route. The reduction in particle size with increase in concentration of PEG is due to the size control effect of PEG molecular structure. The rod-like morphology becomes as an irregular morphology with increase in PEG additives. It was inferred in the present work that the composition of PEG shows significant influence on particle size, thermal stability and antimicrobial activities which facilitate to optimize the composition of composite for particular applications. Nanomaterials are greatly promising in the development

Table 2. Anti inflammatory study of PVA/Hap Nano composite.

Concentration (µg/ml)	Percentage inhibition of nano HAp	Percentage inhibition of nano PEG-20/HAp composite	Percentage inhibition of nano PEG-60/HAp composite
1000	93.00	99.12	97.14
800	93.03	99.12	99.21
400	98.67	99.85	98.45
200	98.57	99.90	99.23
100	98.43	99.14	99.44
50	98.72	98.16	98.72
10	99.25	99.52	94.94

of more valuable orthopedic and dental implants. However, the mechanism of interaction between PEG/nano HAp and biologic systems should thoroughly be investigated in the future and applied in studies using *in vitro*, *in vivo* and preclinical methodologies to validate its use for biomedical applications.

REFERENCES

Ahn ES, Gleason NJ, Nakahira A, Ying JY (2001). Nanostructure processing of hydroxyapatite-based bioceramics. Nano Lett., 1(3): 149-153.

Bertinetti L, Tampieri A, Landi E, Ducati C, Midgley PA, Coluccia S, Martra G (2007). Surface structure, hydration and cationic sites of nanohydroxyapatite: UHR-TEM, IR, Microgravimetric studies. J. Phys. Chem. C., 111: 4027-4035.

Boissiere M, Meadows PJ, Brayner R, Helary C, Livage J, Coradin T (2006). Turning biopolymer particles into hybrid capsules: The example of silica/alginate nanocomposites. J. Mater. Chem., 16: 1178-1182.

Bose S, Saha SK (2003). Synthesis and characterization of hydroxyapatite nanopowders by emulsion technique. Chem. Mater., 15: 4464-4469.

Chen CW, Oakes CS, Byrappa K, Riman RE, Brown K, TenHuisen KS, Janas VF (2004). Synthesis, characterization, and dispersion properties of hydroxyapatite prepared by mechanochemical–hydrothermal methods. J. Mater. Chem., 14: 2425–2432.

Chen DZ, Tang CY, Chan KC, Tsui CP, Yu PHF, Leung MCP, Uskokovic PS (2007). Dynamic mechanical properties and in vitro bioactivity of PHBHV/HA nanocomposite. Compos. Sci. Technol., 67: 1617–1626.

Choi D. Kumta PN (2006). An alternative chemical route for the synthesis and thermal stability of chemically enriched hydroxyapatite, J. Am. Ceram. Soc., 89(2): 444-449.

Darder M, Lo´pez-Blanco M, Aranda P, Aznar AJ, Bravo J, Ruiz-Hitzky E (2006). Microfibrous chitosan-sepiolite nanocomposites. Chem. Mater., 18: 1602-1610.

Degirmenbasi N, Kalyon DM, Birinci E (2006). Biocomposites of nanohydroxyapatite with collagen and poly (vinyl alcohol), Colloids Surf. B: Biointerf., 48: 42-49.

Ding Y, Liu J, Wang H, Shen G, Yu R (2007). A piezoelectric immunosensor for the detection of α-fetoprotein using an interface of gold/hydroxyapatite hybrid nanomaterial. Biomaterials, 28: 2147–2154.

Joseph R, Tanner KE (2005). Effect of morphological features and surface area of hydroxyapatite on the fatigue behavior of hydroxyapatite-polyethylene composites. Biomacromolecules, 6: 1021-1026.

Kannan S, Ferreira JMF (2006). Synthesis and thermal stability of hydroxyapatite-*β*- tricalcium phosphate composites with cosubstituted sodium, magnesium, and fluorine. Chem. Mater., 18: 198-203.

Kannan S, Lemos AF, Ferreira JMF (2006). Synthesis and mechanical performance of biological-like hydroxyapatite. Chem. Mater., 18: 2181-2186.

Lak A, Mazloumi M, Mohajerani M, Kajbafvala A, Zanganeh S, Arami H, Sadrnezhaad SK (2008). Self-assembly of dandelionlike hydroxyapatite nanostructures via hydrothermal method. J. Am. Ceram. Soc., 91(10): 3292-3297.

Li M, Xiao X, Liu R, Chen C, Huang L (2008). Structural characterization of zinc-substituted hydroxyapatite prepared by hydrothermal method. J. Mater. Sci. Mater. Med., 19: 797-803.

Li J, Zuo Y, Cheng X, Yang W, Wang H, Li Y (2009). Preparation and characterization of nano-hydroxyapatite/polyamide 66 composite GBR membrane with asymmetric porous structure. J. Mater. Sci. Mater. Med., 20: 1031–1038.

Ma MG, Zhu YJ, Chang J (2006). Monetite formed in mixed solvents of water and ethylene glycol and its transformation to hydroxyapatite. J. Phys. Chem. B., 110: 14226-14230.

Meenakshi Sundaram N, Girija EK, Ashok M, Anee TK, Vani R, Suganthi R (2006). Crystallisation of hydroxyapatite nanocrystals under magnetic field. Mater. Lett., 60: 761-765.

Murugan R, Ramakrishna S (2004). Bioresorbable composite bone paste using polysaccharide based nano hydroxyapatite. Biomaterials, 25: 3829-3835.

Neira IS, Kolen'ko YV, Lebedev OI, Tendeloo GV, Gupta HS, Guitian F, Yoshimura M (2009). An effective Morphology control of hydroxyapatite crystals via hydrothermal synthesis. Cryst. Growth. Desal., 9(1): 466-474.

Pan Y, Xiong D (2009). Friction properties of nano-hydroxyapatite reinforced poly(vinyl alcohol) gel composites as an articular cartilage. Wear, 266: 699-703.

Pramanik N, Bhargava P, Alam S, Pramanik P (2006). Processing and properties of nano-and macro-hydroxyapatite/poly (ethyleneco-acrylic acid) composites. Polym. Compos., 27: 633-641.

Pramanik N, Mohapatra S, Alam S, Pramanik P (2008). Synthesis of hydroxyapatite/poly(vinyl alcohol phosphate) nanocomposite and its characterization. Polym. Compos., 29: 429-436.

Rajendran V, Nishara Begum A, Azooz MA, El Bata FH (2002). Microstructural dependence on relevant physical–mechanical properties on $SiO_2–Na_2O–CaO–P_2O_5$ biological glasses. Biomaterials, 23: 4263-4275.

Singh MK, Shokuhfar T,. Almeida Gracio JJD, Sousa ACMD, Fereira F, Garmestani H, Ahzi S (2008). Hydroxyapatite modified with carbon-nanotube-reinforced poly(methyl methacrylate): A nanocomposite material for biomedical applications. Adv. Funct. Mater., 18: 694-700.

Wang H, Li Y, Zuo Y, Li J, Ma S, Cheng L (2007). Biocompatibility and

osteogenesis of biomimetic nanohydroxyapatite/polyamide composite scaffolds for bone tissue engineering. Biomaterials, 28: 3338–3348.

Wang M, Li Y, Wu J, Xu F, Zuo Y, Jansen JA (2008). *In vitro* and *in vivo* study to the biocompatibility and biodegradation of hydroxyapatite/poly(vinyl alcohol)/gelatin composite. J. Biomed. Mater. Res. Part. A., 85: 418-426.

Wiria FE, Chua CK, Leong KF, Quah ZY, Chandrasekaran M, Lee MW (2008). Improved biocomposite development of poly (vinyl alcohol) and hydroxyapatite for tissue engineering scaffold fabrication using selective laser sintering. J. Mater. Sci. Mater. Med., 19: 989-996.

Yang JM, Lu CS, Hsu YG, Shih CH (1997). Mechanical properties of acrylic bone cement containing PMMA-SiO$_2$ hybrid solgel material. J. Biomed. Mater Res., 38: 143-154.

Yanbao L, Dongxu L, Weng W (2008). Preparation of nano carbonate-substituted hydroxyapatite from an amorphous precursor. Int. J. Appl. Ceram. Technol., 5(5): 442-448.

Zhan J, Tseng YH, Chan JC, Mou CY (2005). Mimicking the Self-Organized Microstructure of Tooth Enamel. Adv. Funct. Mater., 15: 2005-2009.

Zhang Y, Mild JLA (2008). Efficient biomimetic synthesis of rodlike hydroxyapatite particles with a high aspect ratio using polyvinylpyrrolidone as capping agent. Cryst. Growth Desal., 8(7): 2101-2107.

Zhang W, Liao SS, Cui FZ (2003). Hierarchical self-assembly of nano-fibrils in mineralized collagen. Chem. Mater., 15: 3221-3226.